Journal of Molecular Spectroscopy 348 (2018) 68–78

Contents lists available at ScienceDirect

Journal of Molecular Spectroscopy

journal homepage: www.elsevier.com/locate/jms

High-resolution Fourier transform measurements of air-induced broadening and shift coefficients in the $00^02–00^00$ main isotopologue band of nitrous oxide

Viktor Werwein [a], Gang Li [a], Anton Serdyukov [a], Jens Brunzendorf [a], Olav Werhahn [a], Volker Ebert [a,b,*]

[a] Physikalisch-Technische Bundesanstalt, Bundesallee 100, 38116 Braunschweig, Germany
[b] Centre of Smart Interfaces, Technische Universität Darmstadt, Jovanka-Bontschits-Straße 2, 64287 Darmstadt, Germany

ARTICLE INFO

Article history:
Received 27 April 2017
Accepted 4 July 2017
Available online 8 July 2017

Keywords:
Nitrous oxide
Fourier transform infrared spectroscopy
Spectral line parameters
Air-broadening
Air-shift
Gas metrology

ABSTRACT

In the present study, we report highly accurate air-induced broadening and shift coefficients for the nitrous oxide (N_2O) $00^02–00^00$ band at 2.26 μm of the main isotopologue retrieved from high-resolution Fourier transform infrared (FTIR) measurements with metrologically determined pressure, temperature, absorption path length and chemical composition. Most of our retrieved air-broadening coefficients agree with previously generated datasets within the expanded (confidence interval of 95%) uncertainties. For the air-shift coefficients our results suggest a different rotational dependence compared to literature. The present study benefits from improved measurement conditions and a detailed metrological uncertainty description. Comparing to literature, the uncertainties of the previous broadening and shift coefficients are improved by a factor of up to 39 and up to 22, respectively.

© 2017 Elsevier Inc. All rights reserved.

1. Introduction

In our recent studies, we have determined self-induced broadening and shift coefficients [1] as well as line strengths [2] for the R_0 to R_{40} lines of the $00^02–00^00$-band of the main isotopologue of nitrous oxide ($^{14}N_2{}^{16}O$) using the Voigt-line shape model. The examined band of this greenhouse and major ozone-depleting gas is used by the Total Carbon Column Observing Network (TCCON) [3] to monitor its atmospheric abundance. For its retrievals TCCON utilizes [4] spectral line parameters for the Voigt-profile from the HITRAN-database [5]. The HITRAN line data for air-induced broadening and shift coefficients are based on an extensive FTIR spectroscopy laboratory study of Toth [6] with a nominal spectral resolution of 0.011 cm^{-1} performed over a partial pressure range of air between 389 hPa and 655 hPa.

In Toth's study, results for both collisional parameters measured directly in the $00^02–00^00$-band were reported. An interpolated dataset for the broadening coefficients was also presented, which averages the measured coefficients of several different vibrational bands for the same rotational quantum numbers. Besides, the measured shift coefficients were used to generate a dataset fitted to an empirical model [7]. The mentioned laboratory study is, to the best of our knowledge, the only one concerning air-induced collisional parameters in the TCCON band. Moreover, the given information on the parameter uncertainties is very limited there.

Therefore, the present study aims to provide accurate high-resolution FTIR spectroscopy measurements of air-induced broadening and shift coefficients with the focus on metrological measurement conditions such as pressure, temperature, optical path length and chemical composition as well as on a detailed uncertainty treatment. This complements our N_2O line parameter results mentioned above [1,2] providing a new and highly coherent line parameter set for TCCON remote sensing applications.

2. Experimental details

2.1. Measurement setup

The N_2O in air measurements were carried out in the spectral range from 3800 cm^{-1} to 5200 cm^{-1} using the same setup, based on the high-resolution Fourier Transform spectrometer (FTS) Bruker IFS 125HR at the Physikalisch-Technische Bundesanstalt (PTB), as in our previous studies [1,2]. The nominal spectral resolution is 0.002 cm^{-1} and the nominal beam aperture diameter is 0.5 mm. An optical band-pass filter with a central wavelength of 2.25 μm (full width at half maximum of 0.5 μm) was installed in

* Corresponding author.
E-mail addresses: viktor.werwein@ptb.de (V. Werwein), volker.ebert@ptb.de (V. Ebert).

http://dx.doi.org/10.1016/j.jms.2017.07.002
0022-2852/© 2017 Elsevier Inc. All rights reserved.

the beam path. The residual pressure in the FTS beam path, maintained by two turbo molecular pumps, was significantly below $1 * 10^{-4}$ hPa ensuring a background completely free of parasitic absorptions e.g. due to atmospheric CO_2 or H_2O.

A temperature stabilized custom-made absorption cell placed inside the sample compartment of the FTS and described in Ref. [1] was used. The cell length, measured with a mechanical caliper, amounts to 20.75 cm with an expanded uncertainty of 0.03 cm. The reported uncertainty includes contributions from different orientations of the wedged cell windows to each other as well as path differences between on-axis and off-axis beams under the assumption of a homogenous radial beam intensity. All uncertainties are reported as expanded uncertainties with a coverage factor of $k = 2$ corresponding to a confidence interval of ca. 95%, if not specified otherwise.

The sample pressure was measured with a capacitance diaphragm gauge (MKS Baratron 628D, full scale 1000 Torr) calibrated against the national primary standard of PTB in the range from ca. 15 hPa to 1300 hPa for SI-traceable [8] measurement results. Assuming thermal equilibrium between the cell and the gas, the cell temperature was recorded at three representative positions (body and each of the two window flanges) using precision class 1/10 B Pt100 resistance thermometers. Their accuracy had been verified in the range of 213 K to 308 K via an internal comparison to two PTB Pt100 thermometers in an ethanol bath, which themselves had been calibrated for measurement of temperature traceable to the International Temperature Scale of 1990 (ITS-90) [9].

2.2. Gas samples

The N_2O gas was purchased from AirLiquide with a certified purity of ≥99.999 vol%. The standard air mixture was gravimetrically prepared by the Van Swinden Laboratory [10]. Its metrologically specified N_2 and O_2 amount fractions are 79.107% and 20.893%, respectively, with an absolute expanded uncertainty for both of $3 * 10^{-3}$%. The specified total amount fraction of N_2 and O_2 is 99.99998% with an absolute expanded uncertainty of $9 * 10^{-3}$%. The major specified impurity is H_2O with an amount fraction of $(6 \pm 3) * 10^{-6}$%. No traces of impurities were observed neither in N_2O nor in the air mixture spectra.

2.3. Measurement procedure

The absorption cell and the gas manifold, were evacuated to a pressure of less than $1 * 10^{-3}$ hPa, then purged with N_2O for several times. Hereafter, the N_2O-air mixtures were prepared through manometric addition by filling the cell, first with N_2O up to the desired partial pressure, and then adding the standard air mixture up to the desired total pressure. Passive mixing of the N_2O with air took about one day which was monitored analyzing the spectral absorption profiles as described in Section 3. Two mixtures with a total pressure of 1296 hPa and 723 hPa with an N_2O amount fraction of 20% were prepared. The actual amount fraction of N_2O in the cell volume was determined later on spectroscopically rather than from the respective measured partial pressures. This approach helps to avoid misinterpretation due to imperfect mixing as well as different adsorption or leakage effects of the two gas samples in the absorption cell. Both prepared mixtures served for seven pressure level measurements in total. Pressure and temperature within the cell were monitored continuously during the whole experiment.

In total, a number of 120 to 800 interferograms per pressure level was recorded at 296 K. The initial gas pressure levels were measured for a longer time to monitor the completeness of the mixing process. Measuring each interferogram took 3 min resulting in a total measurement time of about 6 to 45.5 h. Prior to sample measurements background spectra were recorded by co-adding 1560 interferograms (about 81 h) at a total pressure of ca. $1 * 10^{-3}$ hPa.

More details on the measurement setup and procedure are given here [1,2].

3. Data processing and analysis

3.1. Pressure and temperature determination

The effective total gas pressure and temperature, which characterize the measurement conditions, were extracted from the recorded time series. Therefore, the respective time period after sample stabilization was determined. The duration of the selected period amounts typically to 8 hours. The final effective pressure p and temperature T were extracted as the respective temporal average over the selected time window, respectively. Their values and the associated relative expanded uncertainties $U(p)$ and $U(T)$ determined according to the Guide to the Expression of Uncertainty in Measurement (GUM) [11] are summarized in Table 1.

In detail, these uncertainties were calculated by combining the standard uncertainty of the individual measurement point and the standard deviation of the measurand over the selected period. In the case of the temperature the standard deviation over the temporal averages of the different sensors was also considered to account for the spatial inhomogeneity along the cell length. For further details on data processing refer to [1,2]. The obtained relative expanded uncertainty averaged over all pressure levels amounts to less than 0.12% for pressure and less than 0.08% for temperature.

3.2. Spectra processing

The measured interferograms were processed by the FTS software OPUS 7.0 (Bruker). This included averaging of 10 subsequent interferograms corresponding to a measurement time of 30 min, phase correction using the Mertz-algorithm, zero filling with a factor of 2, boxcar apodization and Fourier transformation. Depending on the pressure level the processing yielded 12 to 80 single channel spectra. The sample spectra measured during the selected time period were extracted and averaged to get the effective sample spectrum for each pressure level. Their number was typically 16 (8 h). The corresponding background was calculated by averaging all 156 recorded background spectra (30 min each). Using the averaged spectra and the background the transmission and absorbance of the N_2O-air mixtures were determined. The peak signal-to-noise (S/N) ratio of the analyzed transitions R_0 to R_{40} in the absorbance spectra is in the range between 35 and 500. In Fig. 1, absorbance spectra at 306 hPa, 723 hPa and 1296 hPa of the R-branch are shown exemplarily.

3.3. Determination of the mixing period

The duration of the mixing of the N_2O and the air samples was determined by analyzing the absorption profiles of the spectral

Table 1
Total pressure and temperature as well as their respective relative expanded uncertainties summarized for each pressure level.

p, hPa	$U(p)$, %	T, K	$U(T)$, %
204.03	0.17	296.05	0.08
305.62	0.14	296.04	0.08
506.24	0.10	296.03	0.08
722.81	0.10	296.04	0.08
902.98	0.10	296.02	0.07
1105.27	0.09	296.02	0.07
1295.74	0.08	296.03	0.08

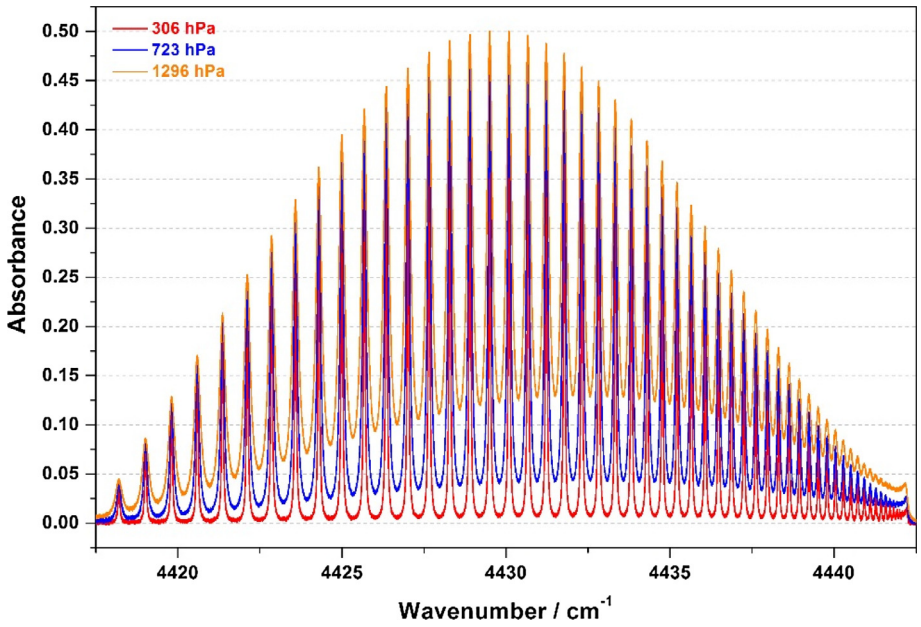

Fig. 1. Measured FTIR-spectra at 306, 723 and 1296 hPa: Observed spectral absorbance in dependence of wavenumber.

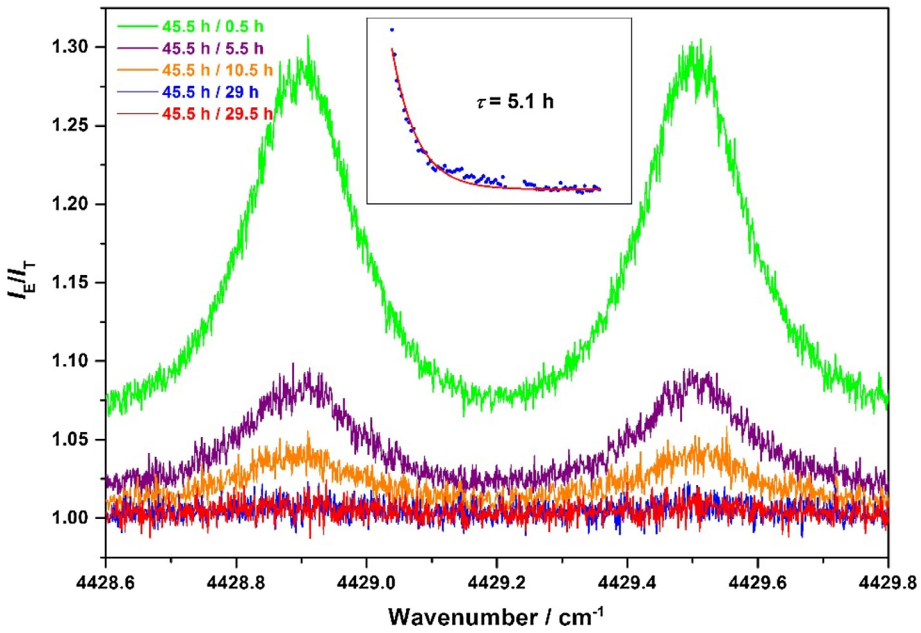

Fig. 2. Ratios of the sample (single channel) spectrum recorded at the end of the pressure level at 1296 hPa to spectra measured at different times after filling the cell exemplarily for the transition region of R_{15} and R_{16}. The embedded graph shows the temporal decrease at the intensity maximum of the R_{16} line.

transitions over up to 45.5 h. These data indicated the mixing to be complete after about one day, since no variations of the line profiles could be observed in the single channel spectra within the noise level after this time duration. Therefore, ratios of the single channel spectrum recorded during the last 30 min I_E (45 h to 45.5 h) to single channel spectra measured during any other different 30 min time slots I_T were calculated: If mixing is complete, then the ratio with and without absorption features is the same (horizontal line) within the noise level. Fig. 2 shows a plot of a couple of ratios of the 1296 hPa pressure level for the region around the two transitions with the best S/N ratio R_{15} and R_{16}. The small embedded graph shows the temporal exponential like decrease at the intensity maximum of the R_{16} line with the decay constant τ.

The ratio at the spectral position of both absorption features decreases significantly within the first hours after filling the cell and then converges to a horizontal line over time, i.e. at the beginning the N_2O concentration in the cell volume is higher than in the manifold. After 28 h this process ends, indicating a complete mixing of the sample. Due to the smaller sample density at 723 hPa total pressure the mixing took less time (21 h).

3.4. Spectra modelling procedure

The transmission spectra were modelled using a new Fortran-based simultaneous multiline fit code developed at PTB [12]. The code employs the HTP fit submodule [13] for the Hartmann-

Tran-profile [14] and its reduced forms. The program applies the non-linear least squares method combined with the Gauss-Newton-algorithm to minimize the sum of quadratic residuals χ^2 between the measured and the model spectrum. For our analysis we used the Voigt-profile, since it is the long-standing spectral line shape model widely used by the remote sensing community and among them by TCCON [4].

During our single spectrum fit procedure the complete R-branch of the $00^02–00^00$-band of $^{14}N_2{}^{16}O$ in the range of 4417 to 4445 cm^{-1} was modelled. Spill-over of closely lying lines from the P-branch and minor bands in a range of 10 cm^{-1} to each side of the fit window was considered. The applied fit strategy was optimized in respect of reducing the degrees of freedom: The Doppler widths of all transitions were calculated from the measured temperature. The individual line areas of the modelled transitions R_0 to R_{40} were calculated using the measured pressure and temperature, the spectroscopically determined amount fraction (see below) and the line strengths values reported by us in Ref. [2]. The Lorentzian widths and line positions for all transitions with line strengths $>1 * 10^{-22}$ $cm^{-1}/(molecule * cm^{-2})$ were fitted. The initial values for the fit were taken from HITRAN [5]. Remaining transitions and the unresolved lines in the band head region were not fitted, but calculated using HITRAN line data. Contributions from spilling over wings of lines lying closely to the fit window were considered by using data from HITRAN.

All lines were fitted simultaneously. No micro window approach was applied. A single baseline described by a second order polynomial and a single sine function with three free parameters (amplitude, frequency and phase) were added to the fit model to account for temporal changes in the background and the channeling effect, respectively. The contribution of the instrumental-line-shape (ILS) function was considered through a convolution of the synthetic spectrum with a numerical ILS, which had been retrieved from a low-pressure spectrum at 1 hPa [2] using LINEFIT 14.5 [15,16].

3.5. Amount fraction determination

By setting the line areas of the analyzed transitions to be fixed model parameters a single bulk parameter directly connected to the area of each spectral line remained free. This is the amount fraction of N_2O. This reduction of the degrees of freedom allowed its spectroscopic determination: An approach of sequential multiple spectra modelling with slightly different specified concentration values was performed. Hereafter, the final χ^2 value of each sequential fit was extracted and modelled with a parabola with respect to the amount fraction. An example is shown in Fig.3 for the 1296 hPa pressure level.

The optimal N_2O amount fraction x_{N2O} was determined from the abscissa position of the parabola minimum. The associated standard uncertainty $u(x_{N2O})$ follows from the parabolic modelling. The fitted amount fraction values and the respective absolute expanded uncertainties $U(x_{N2O})$ are reported in Table 2.

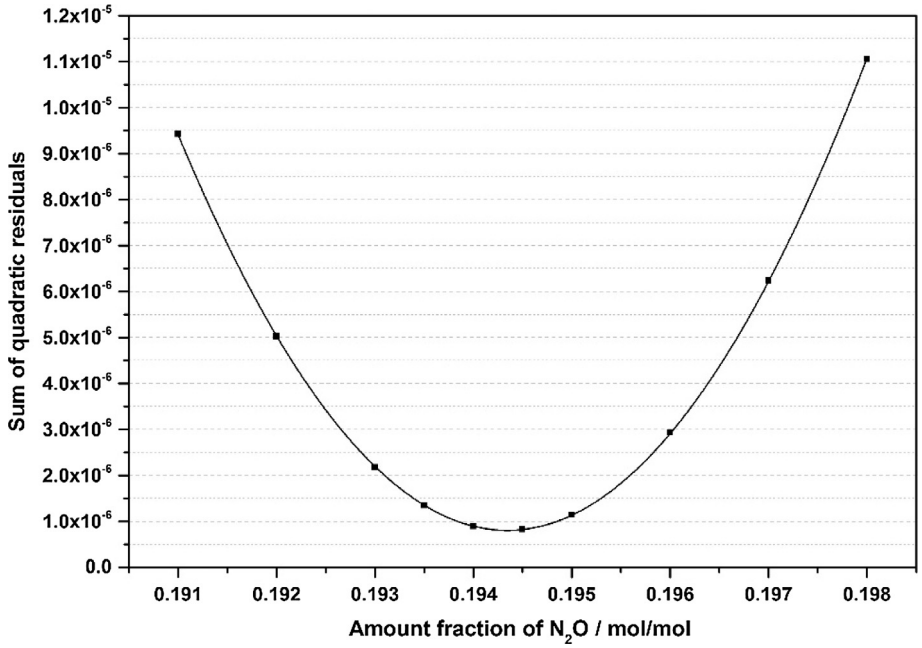

Fig. 3. Modelling of the sum of quadratic residuals with respect to the amount fraction of nitrous oxide for the 1296 hPa pressure level.

Table 2
Spectroscopically determined amount fraction of nitrous oxide, relative difference to manometric determination and partial pressures of nitrous oxide and air together with the respective expanded uncertainties summarized for each pressure level.

Pressure	Fitted amount fraction		Comparison		Partial pressures			
p, hPa	x_{N2O}, mol/mol	$U(x_{N2O})$, 10^{-6} mol/mol	$\Delta(x_{N2O})$, %	$U(\Delta(x_{N2O}))$, %	p_{N2O}, hPa	$U(p_{N2O})$, hPa	p_{Air}, hPa	$U(p_{Air})$, hPa
204.03	0.202395	4	1.3	0.4	41.29	0.07	162.74	0.27
305.62	0.202401	4	1.1	0.4	61.86	0.09	243.76	0.35
506.24	0.195682	6	−1.2	0.3	99.06	0.10	407.18	0.42
722.81	0.199684	2	−0.3	0.3	144.33	0.14	578.48	0.58
902.98	0.193290	5	−2.5	0.2	174.54	0.17	728.44	0.73
1105.27	0.193499	6	−2.4	0.2	213.87	0.19	891.40	0.81
1295.74	0.194345	4	−2.0	0.2	251.82	0.21	1043.92	0.89

A comparison of the fitted with the manometrically determined amount fraction shows relative differences $\Delta(x_{N2O})$ up to 2.5%, which were calculated as the difference between spectroscopically and manometrically determined value divided by the spectroscopically determined value. As mentioned above, the reasons for this should be an imperfectly mixed sample as well as different adsorption and leakage behavior of the individual components.

Using the spectroscopically determined amount fractions and the total pressures from Table 1, the partial pressures of N_2O p_{N2O} and air p_{Air} were determined. Their absolute expanded uncertainties $U(p_{N2O})$ and $U(p_{Air})$ result from the procedure of uncertainty propagation (quadratic combination of $U(p)$ and $U(x_{N2O})$), which holds for all combined uncertainties, if not specified otherwise.

3.6. Spectra modelling results

Using the spectroscopically determined x_{N2O} as fixed input parameter all spectra were reevaluated to determine the broadening and shifting coefficients. The obtained fit residuals calculated as the difference between measurement and model together with their respective global average μ_G and global standard deviation σ_G are shown in Fig. 4. The average of the global standard deviations over all pressures amounts to $1.2 * 10^{-3}$. For the pressure levels from 204 hPa to 903 hPa the individual peak residual structures, calculated as the difference between measurement and model divided by the model value, amount to not more than 1.5% of the absorbance maximum of the respective transition. Most of the obtained residual structures are W-shaped, which is typical for Voigt-profile modelling in the atmospheric pressure range. W-shaped residuals usually arise from the speed dependence of the relaxation rates of the absorber or from the Dicke-narrowing effect. Referring to the results for N_2O-air mixtures in the fundamental band of Loos et al. [17] the W-structure could also be due to speed dependence in this case. Besides the W-structure, small asymmetries of the individual residuals were found. The asymmetry shape tends to be inversely to the R-branch intensity maximum. This indicates a small line-mixing contribution. Line mixing was also found for the fundamental band by Loos et al. [17].

In contrast to the residuals for the pressure levels described above, for the two highest pressure levels of 1296 hPa and 1105 hPa different structures were observed. In these cases, the individual structures in the center of the R-branch all become positive, whereas at the edges of the branch all of them become negative. We interpreted this as a consequence of distinct line-mixing, where intensity is transferred from the far wings to the branch center resulting in a non-satisfying modelling. Since both pressures are above the atmospheric pressure range and, hence, of reduced interest to the remote sensing community, we excluded them from further analysis.

3.7. Determination of air-induced broadening coefficients

The first step to determine the air-broadening coefficient $\gamma_{Air}(T_0)$ is to correct the extracted total Lorentzian widths $\Gamma(T)$ for self-induced collisional broadening contribution using the respective partial pressure of N_2O from Table 2, the respective temperature from Table 1 and self-broadening coefficients $\gamma_{N2O}(T_0)$ from our recent publication [1]. Afterwards, the resulting Lorentzian widths $\Gamma_{Air}(T)$ due to air-induced broadening were converted to the reference temperature of 296 K. In both cases, for the temperature exponent of self- and air-broadening $n(\gamma_{N2O})$ and $n(\gamma_{Air})$ a value of 0.5 within the power law model was used. To account for different possible temperature behavior of the collisional widths the absolute expanded uncertainty of the respective exponent was very conservatively estimated to be 1.5.

To determine γ_{Air} for the R_0 to R_{40} transitions a generalized linear regression (GLR) of the respective Lorentzian width due to air-broadening $\Gamma_{Air}(T_0)$ with respect to the partial pressure of air from Table 2 was performed in the total pressure range from 204 hPa to 903 hPa. Following community standards in spectroscopic databases, the pressure values were converted in units of physical atmospheres with 1 atm = 1013.25 hPa. The air-broadening coefficient of a transition corresponds to the slope of the respective

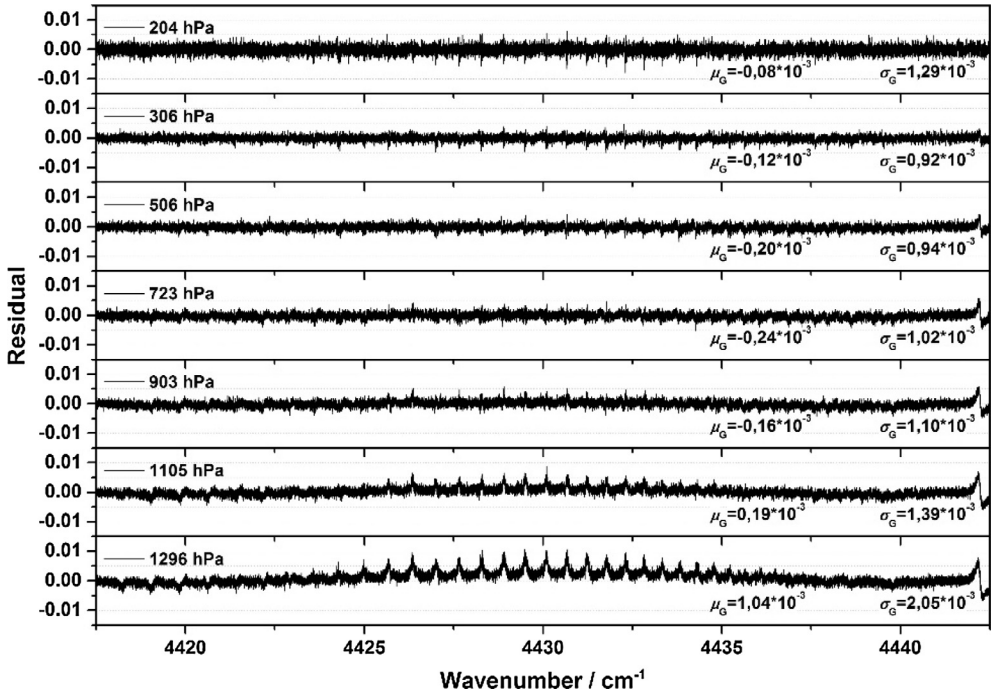

Fig. 4. Modelling of the measured FTIR-spectra: Fit residuals for all seven measured pressure levels.

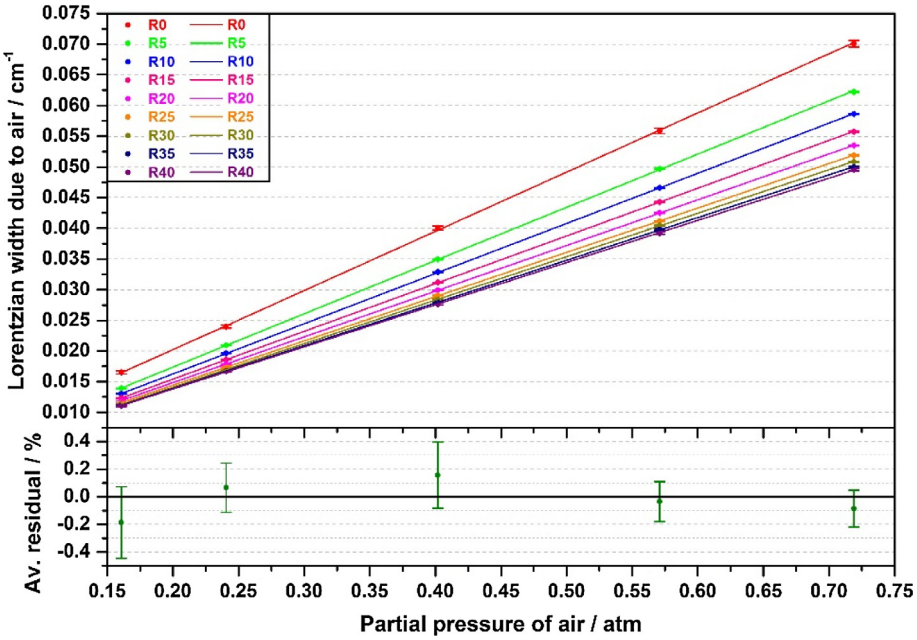

Fig. 5. Upper panel: Generalized linear regressions of Lorentzian widths with respect to the partial pressure of air for selected lines spanning the analyzed spectral window. The Lorentzian widths are depicted with estimated expanded uncertainties. Lower panel: Arithmetic mean of the relative residuals across the transitions R_0 to R_{40} and the respective standard deviation.

Table 3
Relative contributions of the individual data points to the total uncertainty of the air-broadening coefficient representatively for the transitions R_0 and R_{16}.

p_{Air}, hPa	R_0		R_{16}	
	$u(p_{Air})$, 10^{-1}%	$u(\Gamma_{air}(T_0))$, %	$u(p_{Air})$, %	$u(\Gamma_{air}(T_0))$, %
162.74	1.82	23.56	6.36	18.45
243.76	1.59	8.74	0.87	1.77
407.18	0.47	3.49	1.95	5.99
578.48	3.64	22.79	6.02	19.17
728.44	6.91	39.97	10.09	29.34

regression line. GLRs of representative transitions across R_0 to R_{40} are shown in the upper panel of Fig. 5. In the lower panel the average relative residual across all 41 analyzed transitions is depicted. The residual of an individual transition was calculated as the difference between measurement and model divided by the measured value.

The majority of the measurement points is described by the model within the respective expanded uncertainty. All residuals of the linear model averaged over J are less than 0.17%. These low values confirm the suitability of the applied model for the description of air-induced broadening in the atmospheric pressure range. The combined uncertainty of γ_{Air} contains individual contributions from fitting the Lorentzian widths, pressure, temperature and amount fraction determination, self-broadening data and the temperature coefficients of self- and air-broadening as well as the regression procedure. The relative contributions of $u(\Gamma_{Air}(T_0))$ and $u(p_{Air})$ to $u(\gamma_{Air}(T_0))$ depend on the intensity of the spectral line. The contributions of individual regression data points to the total uncertainty are summarized representatively for the weakest and strongest analyzed transition R_0 and R_{16} in Table 3.

The compilation shows that $u(\Gamma_{Air}(T_0))$ is the dominating contribution for weak lines with an relative amount of up to 40%. For the strongest transitions the influence of $u(p_{Air})$ increases significantly up to a value of 10%.

Besides the described uncertainty contributions, the higher order line shape effects as described above might also have caused the slight deviations between the measurement data and the linear model.

3.8. Determination of air-induced shift coefficients

Analog to the air-broadening determination all fitted line positions $\nu_0(T)$ were firstly corrected for self-induced shift contributions with the aid of recently measured self-shift coefficients $\delta_{N2O}(T_0)$ [1]. Following this, GLRs of the corrected line positions due to air $\nu_{0,Air}(T)$ with respect to the temperature weighted partial pressure of air $p_{Air} * (T_0/T)^n(\delta_{Air})$ (cf. Eq. (7) in Ref. [1]) were carried out. In both steps, the power law model for the temperature behavior was applied assuming self- and air-shift temperature exponents $n(\delta_{N2O})$ and $n(\delta_{Air})$ with values of 0.5 [18] and a very conservative stated absolute expanded uncertainty of 1.5. Fig. 6 shows some representative regression examples in the upper panel and the average relative residual across all analyzed transitions in the lower panel. For the purpose of a better illustration, in the upper panel the vacuum position of the respective transition (y-axis intercept of the regression line) was subtracted from the corresponding fitted line positions. For the determination of the relative residuals, the line positions were also corrected by subtracting the respective vacuum position.

Most of the resulting regression lines are within the expanded uncertainty of the measurement data. All averaged relative residuals with respect to the vacuum position corrected line positions are

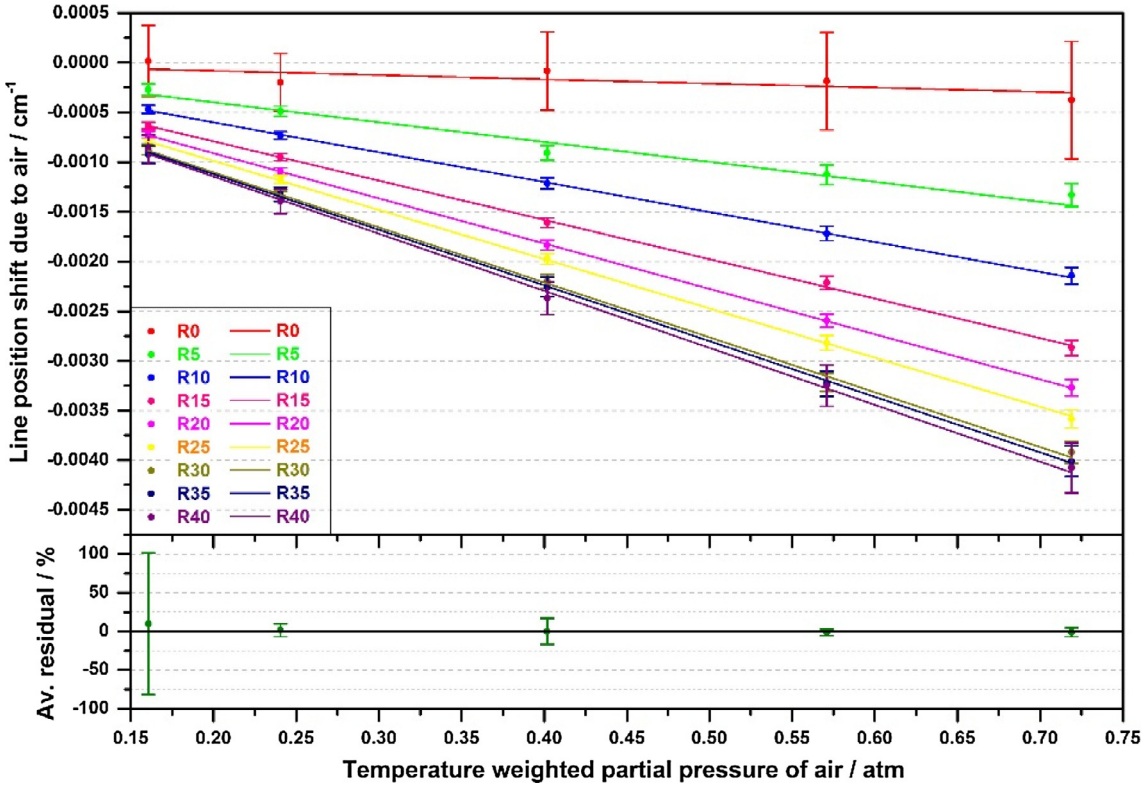

Fig. 6. Upper panel: Generalized linear regressions of line positions with respect to temperature weighted partial pressure term of air for selected lines spanning the analyzed spectral window. The line positions are depicted with estimated expanded uncertainties. For the purpose of a better illustration, the respective vacuum line position was subtracted from the fitted line positions. Lower panel: Arithmetic mean of the relative residuals across the transitions R_0 to R_{40} and the respective standard deviation.

Table 4
Relative contributions of the individual data points to the total uncertainty of the air-shift coefficient representatively for the transitions R_0 and R_{16}.

p_{Air}, hPa	R_0		R_{16}	
	$u(p_{Air})$, 10^{-7}%	$u(\nu_{0,air}(T))$, %	$u(p_{Air})$, 10^{-2}%	$u(\nu_{0,air}(T))$, %
162.74	24.81	23.52	2.37	24.11
243.76	28.81	10.58	0.94	5.10
407.18	6.00	2.66	0.82	6.08
578.48	63.35	22.27	3.46	24.34
728.44	122.94	40.96	6.00	40.23

below 9.8%. The scattering of the residuals at the total pressure of 204 hPa is significantly larger than at higher pressures. This is mainly caused by a shorter measurement time and the small absolute shift contribution primarily for low rotational quantum numbers. Table 4 summarizes individual relative contributions of $u(\nu_{0,Air}(T))$ and $u(p_{Air} * (T_0/T)\hat{}n(\delta_{Air}))$ to $u(\delta_{Air}(T_0))$ for R_0 and R_{16}, representatively. In the case of shift coefficients $u(\nu_{0,Air}(T))$ is by far the dominating contribution to $u(\delta_{Air}(T_0))$, even for the strongest analyzed transitions, although for the latter the contribution of $u(p_{Air} * (T_0/T)\hat{}n(\delta_{Air}))$ increases.

The deviations from the regression model might also have been caused by higher order line shape effects. Especially line-mixing could have affected the results through its asymmetric distortion of the line profile. In our uncertainty budget we studied the variation of the resulting air-shift coefficients in dependence of the regression pressure range. For this, we also performed GLRs in the total pressure range of 204 hPa to 723 hPa and calculated the differences to the original air-shift analysis over the full pressure range. These deviations caused by the modification of the pressure range were treated as a further individual standard uncertainty contribution and combined with the respective standard uncertainty from the original analysis.

4. Results and discussion

4.1. Air-induced broadening coefficients

The air-induced broadening coefficients $\gamma_{Air}(T_0)$ of the rotational quantum numbers $0 \leq J \leq 40$ obtained from the performed GLRs for the reference temperature of 296 K together with their associated relative expanded uncertainties $U(\gamma_{Air})$ are summarized in Table 5. The average relative expanded uncertainty $\mu(U(\gamma_{Air}))$ across all 41 transitions amounts to 0.29% with a spread, i.e. standard deviation $\sigma(U(\gamma_{Air}))$, of ±0.13%.

In Table 5, the relative differences $\Delta(\gamma_{Air})$ between the literature datasets of Toth [6] (cf. Section 1) and this study (calculated as the difference between literature and this study divided by this study) and the respective relative expanded uncertainties $U(\Delta(\gamma_{Air}))$ are also listed. In this context, the uncertainty of Toth's measured values was determined by means of the variation between the results obtained at different sample pressures. The uncertainty of his interpolated values was not reported. The only information given by him regarding the uncertainties is that the coefficients measured with an uncertainty better than 0.002 cm^{-1}/atm were considered exclusively in the interpolation model. The latter value

Table 5
Comparison of air-broadening coefficients with literature data [6] in dependence on rotational quantum number.

J	γ_{Air}	$U(\gamma_{Air})$	$\Delta(\gamma_{Air})$	$U(\Delta(\gamma_{Air}))$	$\Delta(\gamma_{Air})$	$U(\Delta(\gamma_{Air}))$
	This study		Toth interpolation		Toth measurement	
1	10^{-2} cm^{-1}/atm	%	%	%	%	%
0	9.636	0.89	−0.60	4.25	–	–
1	9.262	0.47	1.33	4.34	4.19	7.57
2	9.013	0.35	2.12	4.45	−1.25	13.32
3	8.876	0.29	1.80	4.52	0.05	4.52
4	8.778	0.26	1.16	4.56	1.39	9.12
5	8.683	0.24	0.60	4.61	0.77	9.22
6	8.566	0.23	0.40	4.68	2.15	9.34
7	8.457	0.22	0.20	4.74	1.34	1.20
8	8.373	0.22	−0.20	4.78	−1.12	2.40
9	8.269	0.21	−0.25	4.84	−0.59	2.19
10	8.175	0.21	−0.35	4.90	0.42	1.48
11	8.084	0.21	−0.38	4.95	−1.04	5.94
12	7.997	0.21	−0.39	5.01	−0.96	1.76
13	7.907	0.21	−0.27	5.06	0.04	2.29
14	7.841	0.21	−0.41	5.11	0.24	3.07
15	7.780	0.21	−0.53	5.15	−1.80	1.56
16	7.709	0.21	−0.46	5.19	1.05	1.31
17	7.641	0.21	−0.35	5.24	−0.67	2.63
18	7.564	0.21	−0.07	5.29	−0.18	1.08
19	7.509	0.21	−0.03	5.33	−0.25	2.67
20	7.456	0.21	0.03	5.37	−0.88	1.36
21	7.419	0.21	−0.08	5.40	1.36	1.63
22	7.364	0.21	0.10	5.44	−0.32	1.11
23	7.316	0.22	0.23	5.47	−0.90	3.29
24	7.266	0.22	0.42	5.51	−0.22	4.96
25	7.227	0.22	0.50	5.54	0.59	1.40
26	7.194	0.23	0.53	5.56	0.36	1.14
27	7.163	0.23	0.56	5.59	−1.30	2.80
28	7.153	0.24	0.32	5.60	−1.02	2.81
29	7.123	0.25	0.40	5.62	−1.02	1.43
30	7.090	0.26	0.52	5.65	−1.27	3.68
31	7.049	0.27	0.79	5.68	−1.84	2.57
32	7.023	0.28	0.86	5.70	−1.76	8.55
33	7.008	0.30	0.80	5.72	−4.82	4.29
34	6.995	0.32	0.72	5.73	−3.50	11.44
35	6.966	0.34	0.88	5.75	0.92	5.18
36	6.931	0.37	1.12	5.78	−0.74	2.62
37	6.940	0.40	0.75	5.78	2.30	8.65
38	6.927	0.45	0.69	5.79	−2.27	8.67
39	6.947	0.49	0.17	5.78	0.04	2.92
40	6.874	0.55	1.01	5.85	–	–

and the reported individual uncertainties of the measured coefficients we interpreted here as standard uncertainties. Thus, the average relative expanded uncertainties of his datasets are 4.19% (measurement) and 5.22% (interpolation) with a spread of ±3.31% and ±0.47%, respectively.

The comparison of the different datasets is illustrated in Fig. 7. The upper panel of the illustration compares the air-broadening coefficients with each other, the lower one depicts the relative differences between them. The deviation of the literature datasets to our study averaged across all 41 analyzed transitions amounts to −0.32% (measurement) and 0.36% (interpolation) with a respective spread of ±1.59% and ±0.64%.

The graph shows that, with the exception for the transitions R_{15} and R_{33}, all coefficients agree with each other within the respective expanded uncertainties. Consequently, our study confirms Toth's procedure [6] to average measured coefficients of several different vibrational bands within the given uncertainties. Hence, for N_2O the air-broadening coefficients are independent from the vibrational state of the molecule under the given conditions. Our study complements the existing measurements [6], since measured values for the coefficients of the transitions R_0 and R_{40}, which were missing before, could be provided. Moreover, the previous uncertainties of the coefficients could be reduced by a factor of 5 to 39 (measurement) and 5 to 26 (interpolation).

4.2. Air-induced shift coefficients

The results of our air shift analysis are listed in Table 6. The obtained coefficients $\delta_{Air}(T_0)$ for 296 K exhibit an average relative expanded uncertainty $\mu(U(\delta_{Air}))$ of 15.8% with a spread $\sigma(U(\delta_{Air}))$ of ±39.8%. Both relatively large values arise mainly from the large relative expanded uncertainty $U(\delta_{Air})$ of more than 22% for the six transitions with the lowest J numbers (R_0 to R_5), especially R_0 (248%). This can generally be attributed to the small extent of the line position shift.

Table 6 contains relative differences $\Delta(\gamma_{Air})$ of the literature datasets of Toth [6,7] (cf. Section 1) to our measurements (calculated as the difference between literature and this study divided by this study) and the respective relative expanded uncertainties. Toth determined the uncertainties for his measured coefficients [6] from the variation between the results obtained at different pressures. For the relative uncertainty of his calculated results [7] he reported a J-independent value of 30% and below, without giving further details. The aforesaid numbers were interpreted as standard uncertainties by us. Hence, the average relative expanded uncertainty of his datasets amounts to 23.4% (measurement) and 60% (calculation) with a spread of ±19.7% (measurement).

A graphical comparison of the shift datasets is depicted in Fig. 8. Like in the case of air-broadening, our study complements the

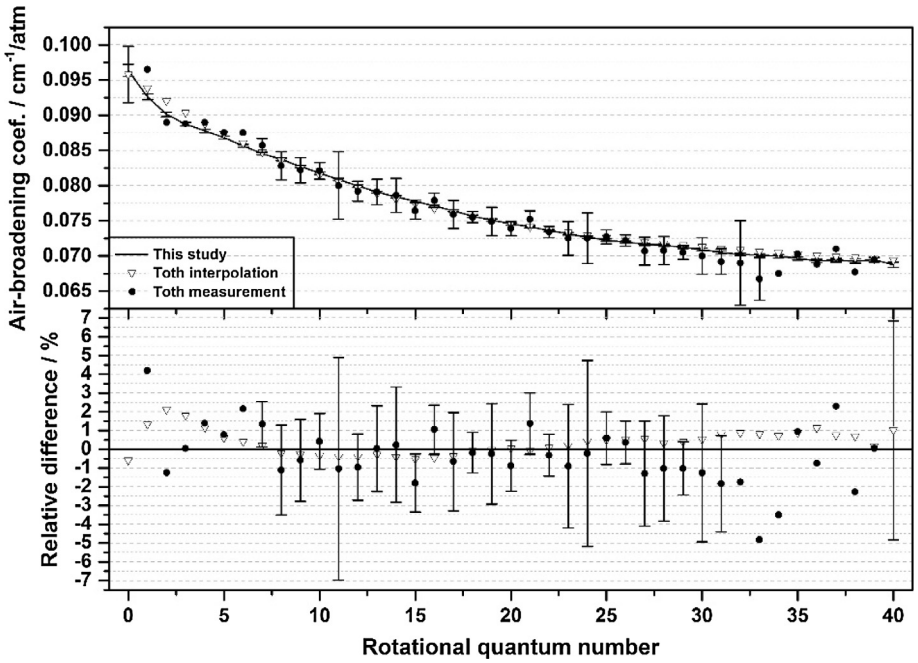

Fig. 7. Comparison of air-broadening coefficients with literature data [6] in dependence on rotational quantum number *J*. Upper panel: Air-broadening coefficients depicted with estimated expanded uncertainties. Lower panel: Relative deviation of the literature data to this study. Uncertainties of the relative deviations are indicated exemplarily.

Table 6
Comparison of air-shift coefficients with literature data [6,7] in dependence on rotational quantum number.

J	δ_{Air}	$U(\delta_{Air})$	$\Delta(\delta_{Air})$	$U(\Delta(\delta_{Air}))$	$\Delta(\delta_{Air})$	$U(\Delta(\delta_{Air}))$
	This study		Toth calculation		Toth measurement	
1	10^{-3} cm^{-1}/atm	%	%	%	%	%
0	−0.419	247.7	654.4	516.0	–	–
1	−0.695	73.3	360.1	285.6	158.8	295.5
2	−1.074	58.6	201.5	190.1	31.3	43.9
3	−1.412	35.3	132.0	143.6	145.8	46.2
4	−1.698	24.7	95.2	119.7	76.1	48.8
5	−1.999	22.4	67.7	103.1	50.1	80.6
6	−2.285	9.3	48.3	89.5	7.2	70.4
7	−2.464	8.8	39.1	83.9	−12.8	25.1
8	−2.635	9.7	31.5	79.5	−11.6	14.7
9	−2.794	8.9	25.4	75.8	8.5	17.9
10	−3.007	5.0	17.7	70.8	−3.2	33.5
11	−3.091	6.9	15.8	69.8	−12.7	17.3
12	−3.375	3.9	7.1	64.4	−18.5	24.0
13	−3.500	5.4	4.4	62.9	7.1	23.1
14	−3.698	3.4	−0.2	60.0	−17.5	16.0
15	−3.958	3.8	−5.8	56.7	−14.6	4.7
16	−3.969	3.2	−5.1	57.0	−12.3	8.6
17	−4.196	3.1	−9.3	54.5	−24.2	14.6
18	−4.366	3.4	−12.0	52.9	−21.0	8.3
19	−4.408	3.1	−12.0	52.9	−11.5	20.6
20	−4.554	2.8	−14.0	51.7	−18.8	5.9
21	−4.683	4.6	−15.5	50.9	−19.9	13.1
22	−4.784	2.7	−16.5	50.2	0.5	12.4
23	−4.856	4.6	−17.0	50.0	−26.9	11.5
24	−4.954	2.9	−17.9	49.4	−20.7	7.4
25	−4.946	3.5	−17.0	49.9	−8.6	26.4
26	−5.089	2.9	−18.6	48.9	−3.3	8.4
27	−5.198	3.5	−19.5	48.4	−10.5	19.5
28	−5.209	3.0	−19.0	48.7	−24.0	15.7
29	−5.197	3.3	−18.1	49.3	−12.8	5.1
30	−5.525	4.8	−22.3	46.9	−22.4	4.3
31	-5.244	8.7	−17.4	50.3	−13.4	11.6
32	−5.564	4.2	−21.5	47.3	−11.0	18.3
33	−5.450	5.3	−19.1	48.8	1.8	7.3
34	−5.593	8.2	−20.5	48.4	−20.4	18.4

Table 6 (*continued*)

J	δ_{Air}	$U(\delta_{Air})$	$\Delta(\delta_{Air})$	$U(\Delta(\delta_{Air}))$	$\Delta(\delta_{Air})$	$U(\Delta(\delta_{Air}))$
	This study		Toth calculation		Toth measurement	
1	10^{-3} cm^{-1}/atm	%	%	%	%	%
35	−5.606	4.7	−20.1	48.2	23.4	36.0
36	−5.678	10.1	−20.4	48.8	6.7	53.0
37	−5.699	6.0	−20.0	48.4	−9.1	32.0
38	−5.825	5.9	−21.1	47.7	−19.3	28.0
39	−5.729	9.2	−19.2	49.4	−36.8	10.9
40	−5.739	8.0	−18.6	49.5	–	–

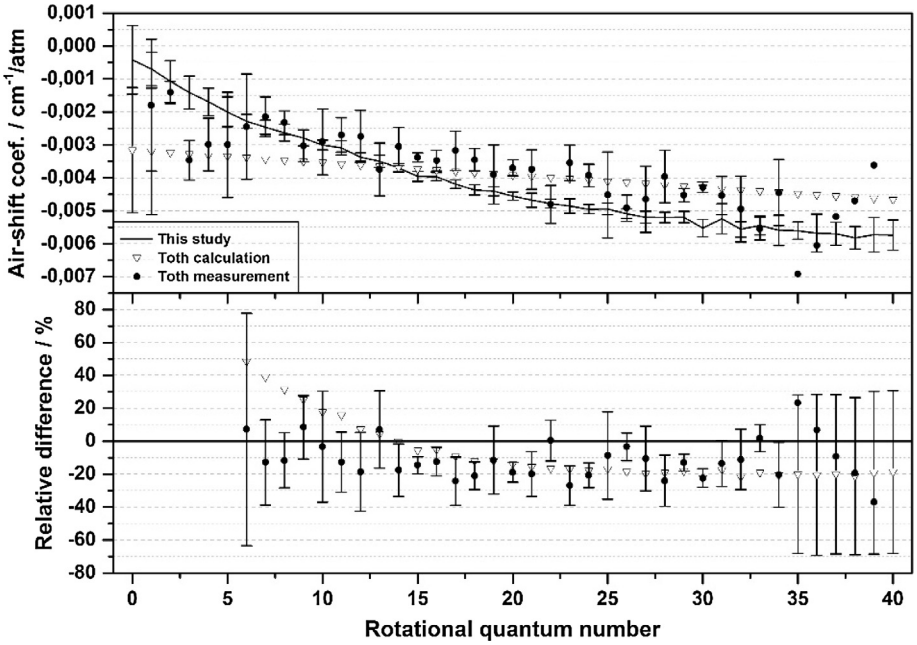

Fig. 8. Comparison of air-shift coefficients with literature data [6,7] in dependence on rotational quantum number J. Upper panel: Air-shift coefficients depicted with estimated expanded uncertainties. Lower panel: Relative deviation of the literature data to this study. Since the differences for small J exceed 100% (cf. Table 6), these are plotted only for the higher J values. Uncertainties of the relative deviations are indicated exemplarily.

measured dataset [6] with results for the transitions R_0 and R_{40}. The comparison, however, shows that both measurements [6] agree only partially within the given expanded uncertainties. For J values of 3–4, 15–18, 20–21, 23–24, 28–30 and 39 they do not match. On the other hand, all of the calculated coefficients [7] agree with our measurements except the transition R_1. But, this is caused by the higher relative uncertainties of the calculated coefficients. Generally, the datasets reported by Toth, especially the calculated one, imply a slower decrease in J dependence than our values. Their average deviation to our measurements is 2.0% (measurement) and 30.8% (calculation) with a spread of ±41.3% and ±123.0%, respectively.

Possible reasons for the observed discrepancies are a limited spectral resolution and the influence of an asymmetric ILS. In this context, our study benefits from the enhanced resolution (factor of 5.5 higher) and state of the art accounting for the ILS of the spectrometer. Especially the spectral resolution plays, here, a crucial role and should be the reason for the relatively strong scattering of the coefficients measured by Toth [6]. As one can see from Table 6, the coefficients for N_2O are small, partly because of the small dipole moment of the molecule. Within the pressure range of Toth's study the shifts are smaller than ca. $4 * 10^{-3}$ cm^{-1}, which itself is a factor of 3 smaller than his spectral resolution of 0.011 cm^{-1} and, thus, difficult to detect accurately.

5. Conclusions

In our study, we measured air-induced collisional broadening and shift coefficients of the 00^02–00^00-band transitions R_0 to R_{40} of $^{14}N_2{}^{16}O$ at 296 K using high-resolution Fourier transform spectroscopy. The coefficients were determined using the Voigt-line shape model in the partial pressure range of air between 123 hPa and 728 hPa. Their average relative expanded uncertainty amounts to 0.29% for the broadening and 15.8% for the shift coefficients with a spread of ±0.13% and ±39.8%, respectively. Our results validate the extensive air-broadening coefficient measurements and interpolation model of Toth [6] within his large and our smaller reported uncertainties. The interpolation model assumes these parameters to be independent on the vibrational state of the molecule. For the shift coefficients, however, we obtained a different rotational dependence than predicted by Toth's empirical model [7], which is the long-standing HITRAN [5] source.

The benefits of our study are a factor of 5.5 higher spectral resolution, the consideration of the ILS contribution with the state of the art method, the robust parameter retrieval method by a generalized linear regression over two times broader atmospheric pressure range, the verified temperature and the metrologically traceable pressure with uncertainties determined according to the GUM [11]. A fundamental improvement is the detailed

uncertainty description including contributions of pressure, temperature, amount fraction, self-broadening and -shift data, temperature exponents of broadening and shift coefficients, the fit and the regression procedure. Nevertheless, in our study the uncertainties of both line parameters were significantly reduced, namely by a factor of 5 to 39 for the broadening and 2 to 22 for the shift coefficients.

Using our recent results on self-induced broadening and shift coefficients [1] as well as line strengths [2] for the determination of air-induced collisional parameters, we generated a new and coherent set of spectral line parameters for the TCCON-remote sensing band of N_2O.

Acknowledgements

The authors are grateful to Dr. Alexandra Lüttschwager for fruitful discussions and proofreading the manuscript. The authors also acknowledge valuable support during the development of the multiline fitting software from Ha Tran and colleagues. The authors acknowledge financial support and collaboration within the framework of the EMRP project EUMETRISPEC. The EMRP is jointly funded by the EMRP participating countries within EURAMET and the European Union.

References

[1] V. Werwein, J. Brunzendorf, A. Serdyukov, O. Werhahn, V. Ebert, First measurements of nitrous oxide self-broadening and self-shift coefficients in the 0002–0000 band at 2.26 μm using high resolution Fourier transform spectroscopy, J. Mol. Spectrosc. 323 (2016) 28–42, http://dx.doi.org/10.1016/j.jms.2016.01.010.

[2] V. Werwein, J. Brunzendorf, G. Li, A. Serdyukov, O. Werhahn, V. Ebert, High-resolution Fourier transform measurements of line strengths in the $00^0 2–00^0 0$ main isotopologue band of nitrous oxide, Appl. Opt. 56 (2017) E99–E105, http://dx.doi.org/10.1364/AO.56.000E99.

[3] D. Wunch, G.C. Toon, J.-F.L. Blavier, R.A. Washenfelder, J. Notholt, B.J. Connor, D. W.T. Griffith, V. Sherlock, P.O. Wennberg, The total carbon column observing network, Philos. Trans. Roy. Soc. Lond. A: Math. Phys. Eng. Sci. 369 (2011) 2087–2112, http://dx.doi.org/10.1098/rsta.2010.0240.

[4] D. Wunch, G.C. Toon, P.O. Wennberg, S.C. Wofsy, B.B. Stephens, M.L. Fischer, O. Uchino, J.B. Abshire, P. Bernath, S.C. Biraud, J.-F.L. Blavier, C. Boone, K.P. Bowman, E.V. Browell, T. Campos, B.J. Connor, B.C. Daube, N.M. Deutscher, M. Diao, J.W. Elkins, C. Gerbig, E. Gottlieb, D.W.T. Griffith, D.F. Hurst, R. Jiménez, G. Keppel-Aleks, E.A. Kort, R. Macatangay, T. Machida, H. Matsueda, F. Moore, I. Morino, S. Park, J. Robinson, C.M. Roehl, Y. Sawa, V. Sherlock, C. Sweeney, T. Tanaka, M.A. Zondlo, Calibration of the total carbon column observing network using aircraft profile data, Atmosph. Meas. Tech. 3 (2010) 1351–1362, http://dx.doi.org/10.5194/amt-3-1351-2010.

[5] L.S. Rothman, I.E. Gordon, Y. Babikov, A. Barbe, D.C. Benner, P.F. Bernath, M. Birk, L. Bizzocchi, V. Boudon, L.R. Brown, A. Campargue, K. Chance, E.A. Cohen, L.H. Coudert, V.M. Devi, B.J. Drouin, A. Fayt, J.-M. Flaud, R.R. Gamache, J.J. Harrison, J.-M. Hartmann, C. Hill, J.T. Hodges, D. Jacquemart, A. Jolly, J. Lamouroux, R.J. Le Roy, G. Li, D.A. Long, O.M. Lyulin, C.J. Mackie, S.T. Massie, S. Mikhailenko, H.S.P. Müller, O.V. Naumenko, A.V. Nikitin, J. Orphal, V. Perevalov, A. Perrin, E.R. Polovtseva, C. Richard, M.A.H. Smith, E. Starikova, K. Sung, S. Tashkun, J. Tennyson, G.C. Toon, V.G. Tyuterev, G. Wagner, The HITRAN2012 molecular spectroscopic database, J. Quant. Spectrosc. Radiat. Transfer 130 (2013) 4–50, http://dx.doi.org/10.1016/j.jqsrt.2013.07.002.

[6] R.A. Toth, N_2- and air-broadened linewidths and frequency-shifts of N_2O, J. Quant. Spectrosc. Radiat. Transfer 66 (2000) 285–304, http://dx.doi.org/10.1016/S0022-4073(99)00167-3.

[7] R.A. Toth, Linelist of N2O Parameters from 500 to 7500 cm−1. <http://mark4sun.jpl.nasa.gov/n2o.html>.

[8] Le Système International D'unités (SI), Bureau international des poids et mesures (BIPM), 2006. See also: <http://www.bipm.org/en/measurement-units>.

[9] International Temperature Scale of 1990. <http://www.its-90.com/>.

[10] EUMETRISPEC: Spectral Reference Data for Atmospheric Monitoring. <http://www.eumetrispec.org/emrp/eumetrispec.html>.

[11] Evaluation of Measurement Data - Guide to the Expression of Uncertainty in Measurement, International Organization for Standardization, 2008. See also: <http://www.iso.org/sites/JCGM/GUM-JCGM100.htm> and <http://www.bipm.org/utils/common/documents/jcgm/JCGM_104_2009_E.pdf>.

[12] G. Li, H. Tran, V. Ebert, A Fortran-Based Multi-Spectrum Parameter Retrieval Code (in preparation).

[13] H. Tran, N.H. Ngo, J.-M. Hartmann, Efficient computation of some speed-dependent isolated line profiles, J. Quant. Spectrosc. Radiat. Transfer 129 (2013) 199–203, http://dx.doi.org/10.1016/j.jqsrt.2013.06.015.

[14] N.H. Ngo, D. Lisak, H. Tran, J.-M. Hartmann, An isolated line-shape model to go beyond the Voigt profile in spectroscopic databases and radiative transfer codes, J. Quant. Spectrosc. Radiat. Transfer 129 (2013) 89–100, http://dx.doi.org/10.1016/j.jqsrt.2013.05.034.

[15] F. Hase, T. Blumenstock, C. Paton-Walsh, Analysis of the instrumental line shape of high-resolution Fourier transform IR spectrometers with gas cell measurements and new retrieval software, Appl. Opt. 38 (1999) 3417–3422, http://dx.doi.org/10.1364/AO.38.003417.

[16] F. Hase, Improved instrumental line shape monitoring for the ground-based, high-resolution FTIR spectrometers of the Network for the Detection of Atmospheric Composition Change, Atmosph. Meas. Tech. 5 (2012) (2012) 603–610, http://dx.doi.org/10.5194/amt-5-603-2012.

[17] J. Loos, M. Birk, G. Wagner, Pressure broadening, -shift, speed dependence and line mixing in the ν3 rovibrational band of N2O, J. Quant. Spectrosc. Radiat. Transfer 151 (2015) 300–309, http://dx.doi.org/10.1016/j.jqsrt.2014.10.008.

[18] J.-M. Hartmann, C. Boulet, D. Robert, Collisional Effects on Molecular Spectra, Elsevier, Amsterdam, 2008.